https://doi.org/10.5194/egusphere-2025-5265
Preprint. Discussion started: 10 November 2025
© Author(s) 2025. CC BY 4.0 License.

Organic Alkalinity modulates pH from the Sea-Surface Microlayer during a mesocosm study

Edgar Fernando Cortés-Espinoza [1], Alisa Wüst[1, 2], Ander López-Puertas[1, 3], Oliver Wurl[1], José Martín Hernández-Ayón[4], Hannelore Waska[1], Mariana Ribas-Ribas[1]

[1]Institute for Chemistry and Biology of the Marine Environment (ICBM), School of Mathematics and Science, Carl von Ossietzky Universität Oldenburg, 26129, Germany
[2]Institutionen för Marina Vetenskaper (IMV), Naturvetenskapliga fakulteten, Göteborgs universitet, Gothenburg, 405 30, Sweden
[3]Instituto Universitario de Investigación Marina (INMAR), Universidad de Cádiz, 11510, Puerto Real, Cádiz, Spain
[4]Instituto de Investigaciones Oceanológicas (IIO), Facultad de Ciencias Marinas, Universidad Autónoma de Baja California, 22860, Mexico

Correspondence to: Edgar F. Cortés-Espinoza (edgar.fernando.cortes.espinoza@uni-oldenburg.de)

Abstract. The ocean plays a central role in climate regulation by exchanging carbon dioxide (CO_2) with the atmosphere. This exchange depends on the transfer efficiency across the air-sea boundary layer, the sea-surface microlayer (SML) known to be an organic-rich boundary with a thickness of less than 1 mm. The parameters dissolved inorganic carbon (DIC) and total alkalinity (TA) describe the state of the marine carbon system (MCS). However, organic alkalinity (OA), which arises from weak acid-base functional groups in dissolved organic matter, remains poorly constrained. It is known to modulate pH in organic-rich environments. Yet, to our knowledge, it has not been quantified directly in SML before. Here, we show that the enrichment of OA in the SML modulates pH and that its effect propagates further down into the underlying water (ULW). We track the evolution of the MCS during a 35-day mesocosm study where we induced a phytoplankton bloom. Three distinct bloom phases were identified by different biological processes dominating within the system. Dissolution dominated during the pre-bloom phase; photosynthesis and calcification prevailed during the bloom; and CO_2 invasion, together with respiration, was most pronounced in the SML during the transition to the post-bloom phase. These processes provided the context for the observed variability in OA. We measured OA directly by differential potentiometric back-titration as a second titration on the same titrated TA samples. OA in the SML was persistently enriched (Enrichment Factor (EF) > 1) and reached concentrations up to 264 µmol kg⁻¹. On average, it contributed 8.4% of TA, compared to 3.1% in the ULW. Concurrently, the vertical pH differences between SML and ULW decreased towards zero as the bloom began and occasionally became negative. Over the study period, OA EF and ΔpH were negatively correlated (Spearman ρ = -0.75, p = 0.024), indicating that stronger OA EF dampens the pH rise associated with the bloom onset and its effect propagates further down to the ULW. Recognising that OA enrichment modulates pH in both the SML and the ULW, routine inclusion of OA in near-surface measurements and a three-layer air-SML-ULW framework should guide future evaluations of air-sea CO_2 exchange.

https://doi.org/10.5194/egusphere-2025-5265
Preprint. Discussion started: 10 November 2025
© Author(s) 2025. CC BY 4.0 License.

1 Introduction

The ocean is the largest active carbon reservoir on Earth, regulating the planet's climate through the exchange of carbon dioxide (CO_2) with the atmosphere (Friedlingstein et al., 2025). Traditional approaches to assessing air-sea CO_2 exchange have primarily concentrated on near-surface waters (3–5 m), relying on the principal marine carbon system (MCS) parameters, including dissolved inorganic carbon (DIC), total alkalinity (TA), and pH (Bakker et al., 2014; Takahashi et al., 2009). These approaches often neglect the low contribution of organic matter to the MCS (Dickson, 2007; Orr et al., 2005; Zeebe and Wolf-Gladrow, 2001). Nevertheless, mounting evidence suggests that the magnitude of air-sea exchange depends on the efficiency of transfer across the ocean's top skin (Pereira et al., 2016; Ribas-Ribas et al., 2018), commonly referred to as the sea-surface microlayer (SML). Functioning as a biogeochemical microreactor boundary, the SML (<1 mm) is consistently enriched in surface-active organic material relative to the underlying water (ULW) (Wurl and Holmes, 2008; Wurl et al., 2011). Multiple studies show that biologically derived organic acids and bases can contribute a non-negligible fraction of TA and thereby modulate pH in productive, organic-rich marine environments (Cai et al., 1998; Hernández-Ayón et al., 2007; Kim and Lee, 2009; Muller and Bleie, 2008). Together, the evidence suggests that assessments of the SML's role in air-sea CO_2 exchange require particular attention to the organic acid-base system, given its potential to modulate pH in seawater.

The seawater acid-base system is maintained primarily by carbonate species from DIC: bicarbonate (HCO_3^-) and carbonate (CO_3^{2-}), and together account for most of the TA (Dickson, 1981; Millero et al., 1993). In addition, TA contains a biologically derived fraction, termed organic alkalinity (OA), which arises from weak acid and base functional groups carried by dissolved organic matter (Cai et al., 1998; Hernández-Ayón et al., 2007; Kerr et al., 2023; Kim and Lee, 2009; Muller and Bleie, 2008). OA is derived from biological processes such as phytoplankton exudation during growth, microbial transformation of exudates, and degradation of organic matter; Typical contributors include acidic exopolysaccharides rich in uronic acids and sulfate, humic-like substances with carboxylate and phenolic groups, and amine-bearing peptides and amino acids (Kuliński et al., 2014; Middelburg et al., 2020; Passow, 2002; Song et al., 2023). Bloom composition matters for DIC and TA from the organic perspective. *Emiliania huxleyi* consume HCO_3^- to form coccolith and produces acidic polysaccharides associated with dissolved oranic matter, whereas diatoms. From diatoms, *Cylindrotheca closterium*, release organic material relaterd to carboxylate-rich extracellular polymeric substances (Alldredge et al., 1993; Paasche, 1962; Passow, 2002). Accordingly, studies have assessed pH modulation by OA in biologically active marine environments.

Across field and experimental observations, OA concentration ranges near zero in offshore waters to several tens of µmol kg^{-1} in coastal and estuarine settings and with a bias in the MCS parameters calculations. OA measurements along the Norwegian coast resolve ~2 to 22 ± 3 µmol kg^{-1} (Muller and Bleie, 2008), 0.1 ± 5.0 µmol kg^{-1} outside plume waters, 16.0 ± 25.4 µmol kg^{-1} in Tampa Bay, and 33.6 ± 18.0 µmol kg^{-1} in the Suwannee River estuary (Yang et al., 2015). Regionally, the Baltic Sea shows that OA contributes ~1.5 to 3.5% of TA, and omitting OA can bias the computed pH (Kuliński et al., 2014). Across river-to-coast transitions OA concentrations ranges from µmol kg^{-1}, with the largest concentrations observed upstream, where humic substances predominate (Song et al., 2023). In laboratory cultures and mesocosm, microalga organics contribute OA up

https://doi.org/10.5194/egusphere-2025-5265
Preprint. Discussion started: 10 November 2025
© Author(s) 2025. CC BY 4.0 License.

to ~15 µmol kg^{-1} (Hernández-Ayón et al., 2007; Ko et al., 2016). These findin so report that omitting OA at these concentrations can misestimate the calculation of other parameters of the MCS like pH, which a bias can be presented by ~0.03 to 0.26 pH (30 to 1590 µatm pCO_2), and by up to ~0.78 pH at low salinity (Kerr et al., 2023; Ko et al., 2016; Kuliński et al., 2014).

The SML functions as a biologically active boundary where organic matter accumulates. Enrichment factor (EF) range from ~1.2 to >10, corresponding to concentrations from slightly elevated to more than an order of magnitude higher than in the ULW (Wurl and Holmes, 2008; Wurl et al., 2011). Defined by this enrichment, the SML functions as a chemically and biologically distinct microenvironment in which SML processes can modify local air-sea exchange. Field and tank studies show that surface-active materials in the SML reduce gas-transfer velocities and may alter CO_2 exchange (Moreno-Polo et al., 2025; Mustaffa et al., 2020; Pereira et al., 2016; Ribas-Ribas et al., 2018). For example, Ribas-Ribas et al. (2018) de monstrated suppressions of CO_2 transfer of up to 63% under s rfa tant-enriched surface film conditions. The SML-resolved MCS measurements indicate distinct chemistry at the SML: multilayer sampling has reported DIC, TA and pCO_2 elevated in the SML relative to waters centimeters below, with lower pH at the surface, while microelectrode profiling shows a micrometer-scale layer with measurable pH structure (Gong et al., 2007; Zhang, 2003). Case s dies in organic-impacted systems found higher SML DIC levels than those below, underscoring the near-surface anomalies relevant to pH (Benson, 2015). However, despite this focus on the SML, OA has to our knowledge, not been assessed in terms of its implications for the acid-base system and air-sea CO_2 exchange.

Despite its relevance, OA has been overlooked in near-surface assessments and is absent from most air–sea CO_2 exchange frameworks that treat the boundary as a two-layer system (Ribas-Ribas et al., 2018). Yet, the SML concentrates organic matter, particularly during phytoplankton blooms (Wurl and Holmes, 2008; Wurl et al., 2011), and OA at concentrations of tens of µmol kg^{-1} can influence pH and, consequently, the air-sea exchange of CO_2. Bridging this gap is essential for closing the SML carbon budget and refining the representation of ocean-atmosphere coupling in carbon cycle models. As part of the collaboration in the Biogeochemical Processes and Air-Sea Exchange in the Sea-Surface Microlayer (BASS) project, we directly quantified OA in the SML and ULW during a 35-day induced-phytoplankton bloom mesocosm study and tested whether OA enrichment correlates with the vertical pH structure between the SML and the ULW. By combining direct OA determinations with concurrent DIC, TA, and pH measurements, we assessed how o ic-derived alkalinity modulates acid-base conditions in the SML compared to the ULW. We propose a conceptual three-l r framework (air-SML-ULW) that explicitly incorporates OA a th air-sea boundary to improve process understanding and guide future observations of CO_2 exchange in biologically active, organic-rich marine environment.

https://doi.org/10.5194/egusphere-2025-5265
Preprint. Discussion started: 10 November 2025
© Author(s) 2025. CC BY 4.0 License.

2 Methods

2.1 Mesocosm Study Set[up] and Data Collection Strategy

We conducted a 35-day outdoor mesocosm study at the Sea sURface F[acil]ity (SURF; [GE]OMAR Wilhelmshaven), a concrete basin measuring (8.5 m × 2 m × 1 m; ~17 m^3) equipped with a retractable, light-transmissivity roof. This setup allowed us to exclude wind and rainfall during the measurements while maintaining ambient irradiance conditions. The basin was filled with natural seawater from the adjacent Jade Bay, which was pre-treated by fleece filtration, protein skimming, and flow-through UV to reduce particle load and biological activity. Gentle circulation was maintained using bottom-mounted pumps to prevent sedimentation of the phytoplankton while preserving a quiescent surface. Before [beg]in of the time series, the surface was skimmed w[ith] a glass plate technique (Harvey and Burzell, 1972) to remove residual films. The experiment ran from 15-May to 16-June 2023, with r[egu]lar replenishment of evaporative/sa[mpl]e losses. Bloom p[has]es were defined from chlorophyll-*a*: pre-bloom (18 to 26-May), bloom (27-May to 05-June), and post-bloom (05 to 17-June). To trigger and shape the bloom, inorganic nutrients were added on 26-May, 31-May, and 01-June to achieve a Redfield-like N:P rati[o] (~16.7), with concurrent silicate puls[es]. These additions rapidly e[leva]ted chlorophyll-*a* levels and shifted co[mmu]nity composition. Microscopy and optical proxies identified a mixed haptophyte–diatom bloom d[omi]nated by coccolithophores (*Emiliania huxleyi*) and the diatoms (*Cylindrotheca closterium*) reported by [Bin]i et al. (2025).

2.2 Continuous pH data col[lec]t[i]on from the SML and the ULW

pH was continuously monitored [in] both layers using electrode-based sensors. For the SML, micro-pH sensors (Unisense, Denmark; tip diameter 180 to 220 µm) were mounted upside down with the tip pointing upwar[d]. P[ro]filing across the air–water boundary from 3 mm above the surface to 7 mm below. Each vertical micro-profile was completed in approximately every 40 min. Values representative of the SML were subsequently extracted following the procedure described by Rauch et al. (2025 [sub]mitted to the current special issue), ensuring [that] only data reflecting the SML were collected. SML pH data presented here represent the mean of measurements acquired within ± 1 h of the scheduled sampling time. For the ULW, the CTD48Mc was also equipped with a pH electrode logged at 10-minute intervals and presented here as a continuous data time series only. Both instruments were calibrated with NIST (formerly NBS) aqueous buffers at pH 4.00, 7.00 and 10.00 (Carl Roth; nominal ± 0.01 at 20 °C), with temperature corrections applied to ~25 °C in laboratory conditions. Thus, raw electrode readings are on the NBS/IUPAC scal[e].

2.3 Discrete Sampling and direct measurements of DIC, TA and OA fro[m t]he SML and ULW

For the discrete sampling, given the restr[ict]ed SML daily volume from SURF and a multi-user sample demand (BASS), SML discrete sampling for DIC, TA, and OA was performed every third day to avoid compromising the SML conditions over the study; by contrast, ULW (DIC, TA, OA) was sampled daily. The SML samples were collected using the glass-plate technique (Harvey and Burzell, 1972). A pre-cleaned glass-plate was immersed in the mesocosm study seawater, moved away from the

https://doi.org/10.5194/egusphere-2025-5265
Preprint. Discussion started: 10 November 2025
© Author(s) 2025. CC BY 4.0 License.

perturbed layer, and withdrawn vertically at a controlled speed (~5 cm s^{-1}), allowing a thin film of SML water to adhere. The film was then wiped into a 30 mL borosilicate bottle for DIC analyses and a 100 mL bottle for TA analyses, together with OA. The ULW was sampled simultaneously at a depth of 0.4 m by creating a gentle suction flow through a clean syringe tubing assembly, which enabled us to collect the ULW and transfer it to a 250 mL borosilicate bottle for DIC, TA, and OA analysis. To prevent biological alteration in the samples, each bottle was sealed and poisoned immediately with a saturated mercuric chloride ($HgCl_2$) solution (0.02% of the bottle volume) and stored in the dark at room temperature until analysis was performed (Dickson, 2007).

The DIC concentration was determined coulometrically (CM5017, UIC, IL, USA), following the method described by Johnson et al. (1985) and the recommendations from best-practice guides (Dickson, 2007). A 2.5 mL aliquot of each sample was accurately acidified with 2 mL of 0.1 M H_3PO_4 in a closed acidification module to convert all inorganic carbon species into CO_2 gas. High-purity Alphagaz N_2 (99.999%, Air Liquide, DUS, Germany) flow (100 mL min^{-1}) swept the evolved CO_2 through an Ag_2SO_4 column to remove impurities and then passed into a closed coulometric titration cell containing carbon cathode solution over a carbon anode solution for quantitative absorption, and the coulometer's photometric endpoint was used for charge integration. There, CO_2 was titrated electrochemically and the charge was integrated, with endpoint detection by dual-beam photometry. Certified Reference Materials (CRMs, batches 191, 198, and 209), manufactured by the laboratory of Andrew Dickson (Scripps Institution of Oceanography, CA, USA) were routinely analysed to ensure traceability and precision. Quality control checks were performed after every ten discrete sample measurements, and the results consistently remained within ± 3 µmol kg^{-1} analytical uncertainty.

The TA concentration was directly measured by high-precision closed-cell potentiometric titration (916 Ti-Touch, Metrohm, Switzerland), using protocols aligned with Dickson (2007) with an Aquatrode Plus with Pt1000 (Metrohm AG, Herisau, Switzerland) in a thermostated 25 °C water bath; the lidded cell had ports for the acid syringe, N_2 inlet (with vent needle), electrode, and stirrer to maintain a CO_2-free headspace. A monotone equivalent-point routine (5 µL steps) and drift-controlled acceptance were used. Samples were titrated with certified 0.1 M HCl in 0.6 M NaCl to a potential of +225 mV (approximately pH 3 at 24.6 to 25.0 °C) while continuously purging with N_2 (99.999%) to strip CO_2 and stabilise readings. A 10-min pre-equilibration ensured stability of electrode readings. The titration employed a monotone equivalent-point routine with ~5 µL steps (following method optimization) and drift-controlled acceptance. Stirring and acid delivery were arranged to disperse the acid away from the electrode and prevent bubble accumulation. TA was then estimated from electrode magnetic force and HCl volume data using a Gran function evaluation. The workflow incorporated Dickson CRM (Batches 198 and 209) for daily accuracy checks and applied a CRM-based correction factor. Results remained within ± 3 µmol kg^{-1} analytical uncertainty throughout.

The OA concentration was determined directly after TA was measured, using the same sample (from which all carbonate species had been purged), denoted as base titration. By then, a precise aliquot of 80 µL of 2 M NaOH (prepared by dissolving NaOH (35 g) in 0.6 M NaCl solution) is added to raise the pH close to the initial value; after equilibration, a second titration to the same endpoint was performed again keeping a steady N_2 flow and a stable 25 °C bath. OA was then computed from the electrode

https://doi.org/10.5194/egusphere-2025-5265
Preprint. Discussion started: 10 November 2025
© Author(s) 2025. CC BY 4.0 License.

magnetic force-volume data (Gran evaluation) by subtracting inorganic alkalinity contributions, such as borate (BO_4^-), phosphate (PO_4^{3-}), silicate (Si), sulphate (SU), hydroxide (HO^-), sulphide (SA), fluoride (F), and free protons (H), computed as the following equation:

$$OA = TA - (BO_4^- + PO_4^{3-} + Si + SU + OH^-) + (SA + F + H) \quad (1)$$

Constants followed the best-practice sets: $K^*_{BO_4^-}$ (Dickson, 1990), $K^*_{PO_4^{3-}}$ (Dickson, 2007), K^*_{HF} (Perez and Fraga, 1987) with F from (Riley, 1965); nutrients concentration were provided as spectrophotometric PO_4^{3-} and $Si(OH)_4$ (Bibi et al., 2025). OA was calculated in MATLAB using a 'Masterfile' containing titrant concentrations, sample mass, salinity, total nutrients, and starting potentials. Sulphide was omitted (oxic conditions). Each day began with duplicate subsamples and titrations, and the results remained within ± 3 µmol kg^{-1} of the analytical uncertainty throughout the analysis.

2.3. Data Analysis

All computations and visualisation were carried out in MATLAB R2021a. To remove physical dilution/concentration effects and isolate biogeochemical signals of the induced bloom, DIC and TA were reported as salinity-normalised variables. Normalisation followed Friis et al. (2003) :

$$N\,X = X\ \times (\frac{S_{ref}}{S_i}) \quad (2)$$

Where: NX represents the normalized parameter (NDIC, NTA); X is the measured concentration in µmol kg^{-1}; S_i refers to the salinity measured on each discrete sampling day (i); and $S_{ref} = 29.243 \pm 0.412$ represents the study's initial salinity as a reference. This procedure, consistent with MCS best practice (Dickson, 2007), removes changes driven solely by physics, allowing NDIC vs. NTA patterns to be interpreted in terms of photosynthesis/respiration, calcium carbonate ($CaCO_3$) calcification/dissolution, and CO_2 invasion/release. Accordingly, we present the NDIC and NTA time series for the SML and ULW, as well as their joint evolution on an NDIC vs. NTA scatter plot, which is plotted against reference process slopes.

pH anomalies were quantified to assess differences between the SML and the ULW over time. For each paired measurement, anomalies were calculated as the difference between the values from both layers as follows:

$$\Delta pH = pH_{SML} - pH_{ULW} \quad (3)$$

where a positive ΔpH value indicates higher pH in the SML and a negative ΔpH indicates lower pH relative to the ULW. To ensure consistency, the time series from both sensors were aligned and averaged to common intervals (10-minute bins), which were later aggregated to daily means as needed. The anomalies were then analysed across bloom phases (pre-bloom, bloom, post-bloom) to determine shifts in the vertical pH anomalies.

The OA time series was analysed in both layers to compare temporal trends. However, due to the sampling strategy, the SML is represented by fewer data points (every third day, also for DIC and ULW), whereas in the ULW, samples were collected at a higher frequency. Additionally, the percentage of the OA fraction of TA, for each sample available and from both layers, was computed as follows:

$$\%OA/TA = (OA \times 100)/TA \quad (4)$$

https://doi.org/10.5194/egusphere-2025-5265
Preprint. Discussion started: 10 November 2025
© Author(s) 2025. CC BY 4.0 License.

providing a metric of OA significance within the MCS. To quantify OA accumulation in the SML relative to the ULW, we computed an enrichment factor (EF) as the ratio of the OA concentration between both layers. Subsequently, histograms, Q-Q plots, and the Shapiro-Wilk test were used to correlate the OA EF with pH normality. Homoscedasticity (equal variances) was evaluated using boxplots and Levene's test. When the assumptions of normality or equal variances were not met, we used a two-tailed Spearman rank correlation to test associations. Spearman's rho (ρ) indicates the strength and direction (-1 to +1 as maximum correlation and zero as no correlation) of the monotonic relationship. While the p-value indicates whether that observed ρ is statistically significant: $p < 0.05$ ($\alpha = 0.05$) the observed ρ is statistically significant, $p \geq 0.05$, the observed ρ could be due to chance.

Due to a negative correlation between pH and OA, we further examined their relationship by performing a second Spearman rank correlation (two-tailed, $\alpha = 0.05$) between ΔpH and the EF of OA. Only days with matching SML and ULW measurements were included (n = 10). The Spearman correlation was chosen to account for potential non-linear monotonic relationships. Additionally, we quantified the relationship by fitting a linear demming regression model of ΔpH against EF. From this regression, we extracted the slope (change in ΔpH per unit EF), the coefficient of determination (R^2), and the associated 95% confidence interval for the slope, along with its p-value. This combination of non-parametric and parametric approaches allowed us to test both the strength and significance of the monotonic association as well as to estimate the rate of change in ΔpH relative to EF. By applying both methods, we aimed to determine whether OA enrichment in the SML could systematically explain variations in ΔpH, thereby revealing potential mechanistic links between OA accumulation at SML and the observed vertical pH anomalies between both layers.

3 Results

This mesocosm study compared the effects of organic alkalinity (OA) on pH in the sea-surface microlayer (SML) and the underlying water (ULW) during three distinct phases of an induced phytoplankton bloom. Bloom dynamics, inferred from chlorophyll-*a* (Chl-*a*) concentrations, provided the temporal framework for the evolution of bloom phases (see Supplement material Figure S1). Low Chl-*a* concentrations characterised the pre-bloom period (18 to 26-May), followed by a sharp increase that defined the bloom phase (27-May to 05-June), dominated by calcifying organism *E. huxleyi*, reported in the current special issue by Bibi et al. (2025), and a rapid decline during the post-bloom phase (06 to17-June). We first identified the dominant biological processes for each bloom phase using salinity-normalised DIC and TA (NDIC, NTA) to establish the background for OA. We then described the evolution of the OA and pH in both layers across bloom phases. Next, we quantified SML accumulation using an OA enrichment factor (EF) and the vertical pH anomaly (ΔpH) between the SML and ULW. Finally, we tested whether OA EF was negatively correlated with ΔpH. Overall, the results showed persistent OA enrichment in the SML. NDIC and NTA exhibited strong bloom phase-dependent variability, reflecting shifts in dominant biological processes across the study. The ΔpH between both layers was reduced and, at times, inverted during transitions at bloom onset

https://doi.org/10.5194/egusphere-2025-5265
Preprint. Discussion started: 10 November 2025
© Author(s) 2025. CC BY 4.0 License.

and decay. These results established the foundation for assessing OA enrichment and its role in modulating the MCS in the SML.

3.1 Dominant biological processes in the SML and ULW across bloom phases.

We identify the dominant biological processes for each bloom phase, providing a background for subsequent OA dynamics. Salinity-normalised DIC (NDIC) and TA (NTA) time series for the SML and ULW (Figure 1a, b) were examined for this purpose. Their joint evolution was expressed as NDIC vs. NTA vectors (Figure 1c) to illustrate the direction and magnitude of the dominant biological process pathways: photosynthesis/respiration, $CaCO_3$ calcification/dissolution, and CO_2 invasion/release. In the pre-bloom phase, NDIC and NTA were high and exhibited weak variability in both layers. In the SML, NDIC was ~2025 to 2180 µmol kg^{-1}, and NTA continuously increased from 2286 to 2435 µmol kg^{-1}. The ULW showed slightly lower NDIC (~2066 to 2128 µmol kg^{-1}) and NTA (~2300 to 2384 µmol kg^{-1}) concentrations. Examination of the NDIC vs. NTA vectors (Figure 1c) shows that the SML clustered at high values, initially positioned between the CO_2 invasion and $CaCO_3$ dissolution directions. Throughout the pre-bloom phase, NDIC and NTA remained at elevated concentrations. The ULW high-resolution data (Fig. 1c) showed no single dominant process occurring, with vectors alternating among photosynthesis, respiration, dissolution, and calcification. In contrast, $CaCO_3$ dissolution appears to have been the dominant process in the SML, likely triggered by the biological processes occurring in the ULW.

During the bloom phase, in the SML, NDIC dropped rapidly from ~2159 µmol kg^{-1} on 27-May to a minimum of 1684 µmol kg^{-1} on 30-May, then recovered to ~1910 to 1995 µmol kg^{-1} by 05-June. In contrast, NTA decreased more smoothly from 2435 to ~1939 µmol kg^{-1}, a net loss of ~500 µmol kg^{-1} (Figure 1a, b). In the ULW, the decline was steadier: NDIC fell from ~2006–2074 µmol kg^{-1} at bloom start to ~1435 to 1500 µmol kg^{-1} by the end of 05-June, while NTA decreased from ~2328 µmol kg^{-1} to ~1913 to 1939 µmol kg^{-1}. The SML responded more abruptly early in the bloom when NDIC fell by 475 µmol kg^{-1} in three days, then recovered to a level of ~250 to 310 µmol kg^{-1}, whereas the ULW NDIC declined steadily during the bloom phase. Photosynthesis and calcification initially dominated both layers during the bloom phase. Nonetheless, only the SML shifted toward CO_2 invasion by 05-June, likely driven by CO_2 produced from coccolithophore calcification. In contrast, ULW vectors remain aligned with intense photosynthesis and calcification throughout, as shown by a stronger TA decline per unit NDIC (Figure 1c). The bloom phase imposed the strongest restructuring of the MCS from the SML.

https://doi.org/10.5194/egusphere-2025-5265
Preprint. Discussion started: 10 November 2025
© Author(s) 2025. CC BY 4.0 License.

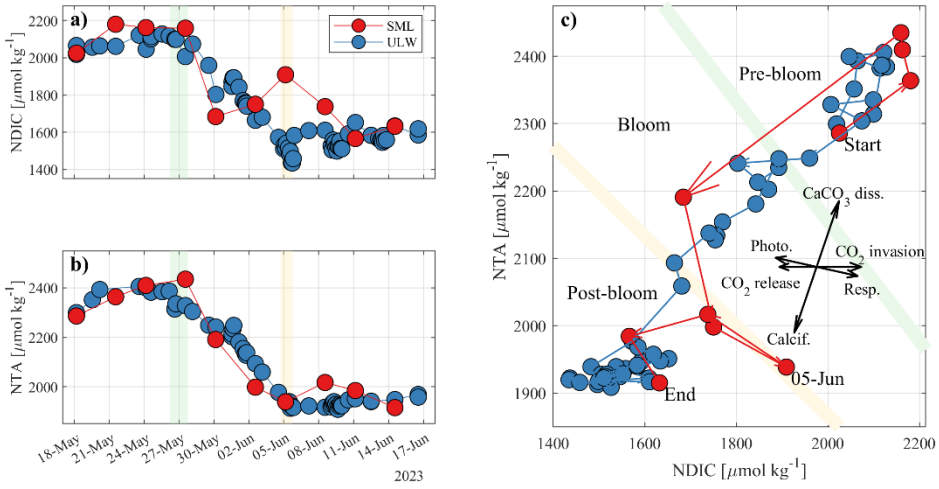

Figure 1: Dominant biological processes in the SML and ULW during bloom phases. (a, b) Salinity-normalised DIC (NDIC) and TA (NTA) for SML (red) and ULW (blue). (c) NDIC vs. NTA scatter plot and showing dominant biological-process vectors: Photosynthesis/Respiration, $CaCO_3$ Calcification/Dissolution, and CO_2 Invasion/Release. Shaded bands indicate the onset of bloom (green) and the transition to bloom decay (yellow).

Finally, at the post-bloom phase in the SML, NDIC decreased from a local maximum near 1909 µmol kg^{-1} (05-June) to 1566 µmol kg^{-1} (10-June), then stabilised around ~1630 µmol kg^{-1} towards the end of the series, while NTA rose briefly to ~2017 µmol kg^{-1} (08-June) before settling between ~1915 and 1985 µmol kg^{-1} (Figure 1a, b). In the ULW, NDIC showed a modest recovery from ~1435 to 1500 to ~1615 to 1620 µmol kg^{-1}, and NTA increased gradually from ~1920 to 1958 µmol kg^{-1}. On the NDIC vs. NTA scatter plot (Figure 1c), SML vectors first align with photosynthesis processes, then rotate towards calcification, and later show respiration signatures; calcification remains superimposed throughout as biomass declines. The ULW exhibited lower NDIC and NTA concentrations, with minor deviations, indicating a trend towards dissolution and CO_2 invasion, accompanied by occasional respiration. In the post-bloom phase, the data remained clustered closely within a narrow range of NDIC and NTA, revealing limited biological activity. Nonetheless, the SML vectors (Figure 1c) varied widely, reflecting shifts between photosynthesis and respiration, with weak but dominant calcification. In contrast, the ULW aligned with CO_2 invasion and weak dissolution. This divergence vector between both layers highlights the SML's dynamic biological response, providing context for OA and pH structure interpretation.

https://doi.org/10.5194/egusphere-2025-5265
Preprint. Discussion started: 10 November 2025
© Author(s) 2025. CC BY 4.0 License.

3.2 Organic alkalinity dynamics and pH evolution in the SML and ULW across bloom phases.

To evaluate the evolution of OA derived by biological processes across the bloom phases in the SML and the ULW, we constructed a time series from the discrete OA measured (Figure 2a). Only at the pre-bloom phase, OA in both layers was comparable, with SML ~110 to 200 µmol kg^{-1} and ULW ~120 to 161 µmol kg^{-1}. On some days, ULW slightly exceeded SML. During the bloom phase, a sharp divergence was observed. SML OA increased to 247 µmol kg^{-1} on 27-May, and then dipped to ~143 µmol kg^{-1} on 30-May, and recovered up to ~180 µmol kg^{-1} by 05-June, when the ULW OA decreased to ~45 to 60 µmol kg^{-1} through this phase. At the post-bloom phase, SML OA rose again, peaking at 264 µmol kg^{-1} on 11-June, then decreased to ~166 µmol kg^{-1} by 14-June, ULW OA remained low and steady at ~43 to 74 µmol kg^{-1}. Thus, SML OA showed a large fraction of the TA (8.1 %) and phase-dependent excursions, while ULW OA had a low fraction of the TA (3.1 %) and was comparatively invariant. The time series showed the accumulation of OA in the SML between bloom phase transitions, which strengthened after bloom onset, whereas the ULW OA remained consistently low and weakly variable.

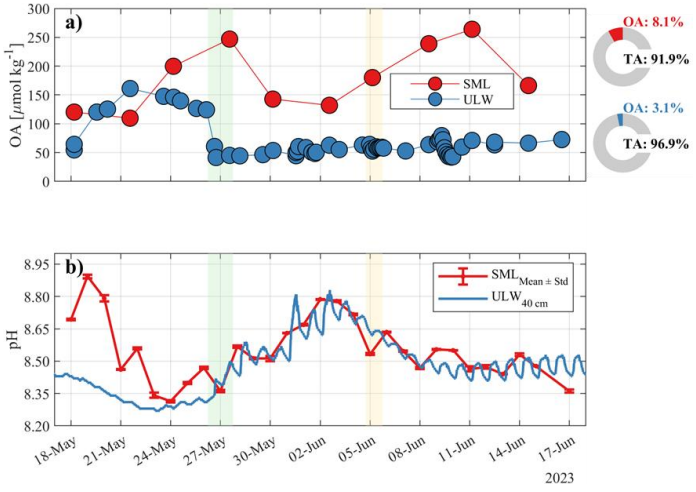

Figure 2: Organic alkalinity (OA) and pH during bloom phases. (a) OA in the SML (red) and ULW (blue) from discrete sampling; right-hand annotations show layer-mean OA fraction to TA over the study period. (b) pH from SML microprofiles (daily mean ± s.d., red), while ULW pH was continuously monitored at 0.4 m (CTD, blue). Shaded bands indicate the onset of bloom (green) and the transition to bloom decay (yellow).

To characterise the vertical pH structure, the SML pH was recorded continuously by microprofiles and averaged to a daily mean ± s.d., while ULW shows continuously monitored of pH at 0.4 m with a CTD-mounted sensor (Figure 2b). In the Pre-bloom, the water column began with a surface-elevated pH state. Nevertheless, SML pH was distinctly higher than the ULW, decreasing from ~8.69 on 18-May to ~8.34 by 24 to 25-May, while ULW pH varied more narrowly from ~8.42 to ~8.31. Bloom phase: ULW pH rose markedly, reaching ~8.75 to 8.80 between 31-May and 05-June, whereas SML pH increased more modestly to ~8.66. During this period, the two records converged and were at times indistinguishable within daily variability. Post-bloom: both layers decreased towards ~8.45 to 8.35. The ULW exhibited small diel oscillations (a few hundredths of a pH unit), whereas the SML showed low-amplitude variability about a similar mean; brief alternations in which layer was

https://doi.org/10.5194/egusphere-2025-5265
Preprint. Discussion started: 10 November 2025
© Author(s) 2025. CC BY 4.0 License.

290 slightly higher were common. Taken together, the progression from an elevated pH in the SML on the pre-bloom to near parity during the bloom phase, followed by minor alternations thereafter at the post-bloom phase, is consistent with the dominant biological processes inferred for each phase and periods of pH decreases coincided with increases in OA (Figure 2a), which provided the reference frame for the subsequent OA pH analysis.

3.3 Organic Alkalinity Enrichment Factor and ΔpH structure between the SML and ULW across bloom phases

295 To quantify SML accumulation, we evaluated the OA enrichment factor (EF) on days with paired measurements between both layers (Figure 3a). Before bloom, EF was generally greater than 1, indicating enrichment at the surface, with an exception on 21-May (EF ≈ 0.68) before rising to 1.37 on 24-May. At bloom onset (27-May), the EF peaked at 5.47, and then decreased to 2.66 by 30-May. During the bloom phase, enrichment persisted (EF ≈ 2.10 to 3.42), and increased again at the bloom-to-post-bloom transition (EF = 3.42 on 05-June) and into early post-bloom (EF = 3.75 on 08-June; 3.71 on 11-June), remaining above
300 2.5 on 14-June. Thus, OA enrichment was strongest at bloom phase transitions (onset and decay) and was sustained at moderate levels thereafter. These results justified the OA fraction to TA ~8.1 % of TA in the SML versus ~3.1 % in the ULW (Figure 2), consistent with persistent SML accumulation. Taken together, the EF record shows that biologically driven OA is selectively enriched in the SML, intensifies during transitions between bloom phases, and remains elevated relative to the ULW across phases, leading to detectable modifications of pH anomalies between the SML and ULW.

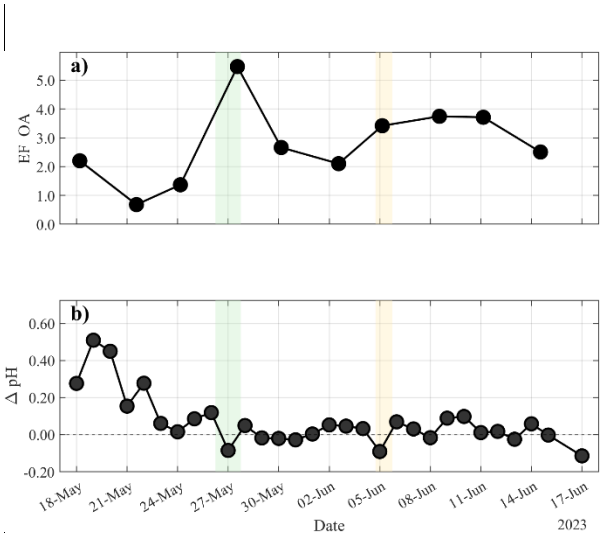

305

Figure 3: OA enrichment and vertical pH anomalies (ΔpH) between SML and ULW during bloom phases. (a) OA enrichment factor, EF = OASML/OAULW; EF > 1 denotes SML enrichment. (b) pH anomaly, ΔpH ≡ pH_{SML} - pH_{ULW} , from daily means. Shaded bands indicate the onset of bloom (green) and the transition to bloom decay (yellow). EF maxima occured at phase transitions, while ΔpH remains near zero or slightly negative values over the same period. SML = sea-surface microlayer; ULW = underlying water.

310 We assessed the vertical pH structure using ΔpH. In the pre-bloom phase, anomalies were consistently positive, with a maximum of +0.51 pH units on 19-May, and declined steadily towards near zero by 24 to 26-May. At bloom onset, ΔpH

https://doi.org/10.5194/egusphere-2025-5265
Preprint. Discussion started: 10 November 2025
© Author(s) 2025. CC BY 4.0 License.

briefly turned negative (-0.085 on 27-May) and then hovered near zero through 31-May to 4-June, indicating convergence of SML and ULW pH during peak bloom activity. A second negative excursion occurred at the bloom-to-post-bloom transition (-0.091 on 05-June). The post-bloom period was characterised by minor, alternating anomalies, generally within ± 0.10, with a more negative value on 17-June (-0.115). Thus, large positive pH anomalies prevailed initially, but they decreased below zero at the transitions between the phases and remained at low amplitudes thereafter. This progression, from elevated pH in the SML's pre-bloom phase to minimal or inverted anomalies at transitions, to small oscillations post-bloom, is consistent with the phase-specific biogeochemical regime inferred from the biological processes. The timing of anomaly minima alongside OA peaks provides a natural framework for testing whether SML OA enrichment is associated with the reduction of the pH difference between the SML and ULW, as examined next.

3.4 Organic Alkalinity Enrichment versus vertical pH anomalies

To evaluate whether OA enrichment at the SML is related to the vertical pH anomalies, we paired it with ΔpH. Given the small sample size and the possibility of a non-linear association, we tested the OA EF vs. ΔpH using both a rank-based (Spearman) test and an ordinary least-squares fit. The OA EF and ΔpH were strongly and inversely related (ρ = -0.75, p = 0.024). The linear Deming regression slope was -0.053 ΔpH units per EF unit. As OA EF increased from near unity to ~4 to 5, the ΔpH between the SML declined by ~0.15 to 0.25, consistent with the reduction of the vertical differences in pH between both layers. Threshold behaviour was evident as: EF > 3 was consistently associated with ΔpH ≤ 0. Taken together, the rank correlation, the negative regression slope, and the magnitude of the implied changes indicate that high SML OA enrichment modifies the vertical pH anomalies between the SML and the ULW. These results show that the ΔpH between both layers typically varies by only 0.02 to 0.05 pH units per day. Nevertheless, when OA EF in the SML increased, ΔpH shifted by ~0.15 to 0.25 pH units. That change exceeds the typical daily variability.

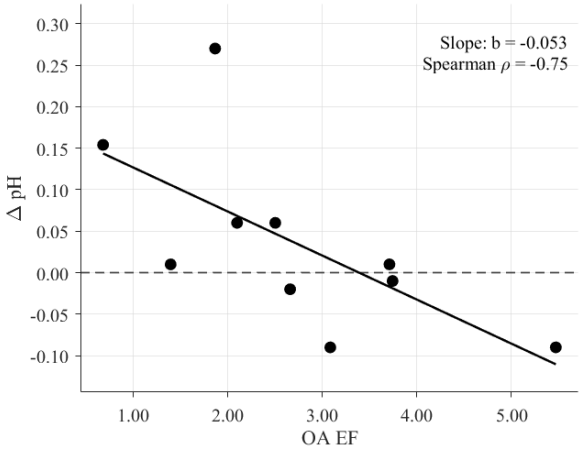

https://doi.org/10.5194/egusphere-2025-5265
Preprint. Discussion started: 10 November 2025
© Author(s) 2025. CC BY 4.0 License.

Figure 4: Spearman negative correlation ρ = -0.75 (p = 0.024) between SML OA enrichment and the vertical pH anomaly. Dashed line marks ΔpH ≡ pH_{SML} - pH_{ULW} plotted against OA EF ≡ OA_{SML}/OA_{ULW}. Solid line represents the linear deming regression model (Slope: b= -0.053 ΔpH per OA EF unit; n = 10).

We interpret this negative correlation between the OA EF and ΔpH in conjunction with phase-specific MCS biological processes that dominate across bloom phases. OA EF maxima occurred at bloom onset and decay, when NDIC vs. NTA vectors showed a switch in the dominant biological processes, and when ΔpH reached its minima. Across the study, OA comprised, on average, ~8 % of TA in the SML (versus ~3% in the ULW), and OA EF remained >1 throughout. The temporal co-occurrence of OA and pH is coherent with the broader MCS evolution: pre-bloom provided a high, buffered baseline system; the bloom imposed a strong drawdown with ULW calcification dominant and SML processes changing from photosynthesis and calcification toward CO_2 invasion and respiration; the post-bloom phase, weaker processes produced minor, alternating pH differences. Within this framework, the variability of OA enrichment within the SML during biologically active transitions between bloom phases is associated with damping, and at times reversing, the SML and ULW pH anomalies. The negative OA EF vs. ΔpH slope integrates this relation across days and bloom phases, linking SML OA peaks at transitions between bloom phases to transient reductions in surface pH that can propagate further down into the ULW. These results lay the groundwork for discussing the mechanisms and implications of near-surface MCS and air-sea CO_2 exchange.

4 Discussion

The OA in the SML remained consistently enriched relative to the ULW throughout the experiment, reaching EF values up to ~5.5 (Figure 3a) and contributing up to ~8 % of TA in the SML compared to ~3.1 % in the ULW (Figure 2a). This enrichment coincided with variations in the vertical pH anomalies between the SML and ULW: as OA EF exceeded ~3, ΔpH between the SML and ULW narrowed toward zero and occasionally inverted. The relationship was captured by a significant negative correlation (ρ = -0.75, p = 0.024; Figure 4), indicating that proton-active organic compounds accumulated at the SML influenced the acid-base balance across bloom phases. SML OA likely contributed to the suppression or reversal of the ΔpH between the SML and ULW. These observations suggest that OA enrichment is not merely a passive product of biological activity but participates in a feedback loop that modulates the interfacial pH. Proton exchange within the acidic and amine functional groups may enhance local buffering, transiently stabilising the pH at the SML. Together, these dynamics identify the SML as a chemically reactive layer with measurable OA influence on the MCS. The observed OA EF and ΔpH dynamics likely result from the sequence of biological processes driving the mesocosm bloom study.

The NDIC vs. NTA vectors revealed a clear sequence of dominant biological processes (Figure 1c): photosynthesis drawdown NDIC at bloom onset, mid-bloom restructuring through calcification, that release CO_2 in the process, and continued photosynthesis, and respiration-driven recovery during decay. During this progression, each phase released and transformed organic matter in the SML. During bloom transitions, when the ΔpH inverted to negative values, the NDIC vs. NTA vectors shifted toward increasing NDIC and decreasing NTA, consistent with respiration and CO_2 release. Guided by prior work on phytoplankton exudates, the released material is likely extracellular polymeric substances, particularly polysaccharides,

https://doi.org/10.5194/egusphere-2025-5265
Preprint. Discussion started: 10 November 2025
© Author(s) 2025. CC BY 4.0 License.

consistent with the observed carbohydrate-like signals (Engel and Passow, 2001; Passow, 2002), humic-like material (Wurl and Holmes, 2008; Wurl et al., 2011), and proteinaceous compounds (Hernández-Ayón et al., 2007; Song et al., 2023). Subsequent microbial processing further enriched proton-active functional groups, enhancing the acid-base system of organics. Under these conditions, OA in the SML remained elevated relative to the ULW and peaked at phase transitions, when biological turnover and organic release were most intense. Collectively, these findings suggest that bloom-driven organic production and transformation transiently amplify the proton reactivity of the SML, allowing OA to modulate pH gradients between the SML and ULW and act as a short-term regulator within the MCS of the mesocosm study.

Mechanistically, these patterns suggest that the phytoplankton bloom supplied organic compounds that contributed to OA in the SML and enhanced their chemical reactivity, influencing local acid-base conditions. The magnitude and timing of OA enrichment suggest that phytoplankton exudation and microbial transformation of organic matter are involved (Engel and Passow, 2001; Passow, 2002; Wurl and Holmes, 2008). Although we did not determine molecular composition here, peaks in OA (Figure 2a) at bloom onset and decay are consistent with intense biological activity. Prior work indicates that extracellular polymeric substances, reported elsewhere to include acidic polysaccharides, humic-like compounds and proteinaceous material, supply proton-active functional groups that can donate or accept protons (Engel and Passow, 2001; Hernández-Ayón et al., 2007; Kim and Lee, 2009; Passow, 2002). Consistent with this mechanism, stronger enrichment (EF $\gtrsim$ 3; Figure 3a) aligned with ΔpH at or below zero, indicating that accumulated proton-active organics can depress pH in the SML and, episodically, in the ULW. These processes align with the NDIC vs. NTA vectors of phase-dominant biological process, which alter the OA pool in the SML.

Previous studies have shown that OA generally remains low. Laboratory cultures and mesocosms yield a few to ~15 μmol kg^{-1}, and in some phytoplankton cultures up to 40 μmol kg^{-1} (Hernández-Ayón et al., 2007; Ko et al., 2016). Field studies across coastal and estuarine systems range from ~0 to 52 μmol kg^{-1} (Cai et al., 1998; Muller and Bleie, 2008; Song et al., 2023; Yang et al., 2015), with Hernández-Ayón et al. (2007) also noting up to 75 μmol kg^{-1} in terrestrially influenced lagoons. In our mesocosm, ULW OA concentrations during the bloom and post-bloom phases ranged from 40 to 100 μmol kg^{-1}, overlapping with and in several cases exceeding the upper limits observed in natural waters. By contrast, the SML maintained higher values throughout the bloom, peaking near 264 μmol kg^{-1} (Figure 2), comparable to the upper coastal estimates inferred from titration fits (46 to 234 μmol kg^{-1}) and to levels in strongly terrestrial-influenced systems (Hernández-Ayón et al., 2007; Song et al., 2023). Our OA EF values are consistent with SML studies of surface-active material, where enrichment spans from ~1.2 to >10 (Wurl and Holmes, 2008; Wurl et al., 2011). Similarly, Bibi et al. (2025), in an accompanying study of this special issue, reported surfactant EF ranging from ~0.5 to 15.3, which are consistent with the magnitude of enrichment observed in our mesocosm.

Methodologically, routine direct OA measurements alongside DIC, TA, and pH supported the interpretation of pH variability across the bloom phases. NDIC–NTA vectors revealed the dominant biological processes governing the system and clarified how bloom-related variability contrasts with the background conditions that shapes OA dynamics. Paired SML and ULW sampling enabled robust comparisons of pH and OA. Reporting OA EF, together with pH anomalies, provides a compact and

https://doi.org/10.5194/egusphere-2025-5265
Preprint. Discussion started: 10 November 2025
© Author(s) 2025. CC BY 4.0 License.

reproducible summary of the layer contrast. For data products and networks, where feasible, providing OA EF and ΔpH values supports consistent assimilation and layer comparison. Conceptually, a three-layer model, air-SML-ULW, clarifies where changes originate and helps avoid attributing pH variability solely to processes below the SML in organic-rich waters. Importantly, SML OA has been overlooked and should be included explicitly. For models and flux observations, we propose including an explicit SML OA term and representing the SML as a distinct, yet potentially unresolved, thin layer with implications for the near-surface MCS. Testing this air-SML-ULW framework in field studies would open a path toward refining representations of air-sea CO_2 exchange and the acid-base system in biologically active marine environments.

In the absence of a certified reference material for OA, accuracy is defined operationally. We established a zero with DOC-free ASW and noted a small but non-zero blank in ASW trials (Appendix B). This approach improves consistency among carbonate system parameters but may retain a small systematic bias in absolute OA. Therefore, interpretations focus on the relative differences between the SML and ULW rather than on absolute concentrations. The temporal resolution was constrained by the SML volume, and discrete SML OA was collected every third day. The chosen sampling frequency resolves sustained bloom phases but may fail to capture short-lived extremes, and therefore may underrepresent the most pronounced deviations in OA EF and ΔpH. Furthermore, the molecular compositions of the organic contributors were not resolved and opens the path for new research. Without identifying the dominant functional groups and their acid-base characteristics, the observed effects cannot be attributed to specific compound classes, which constrains mechanistic interpretation within the SML. Together, these constraints identify clear priorities for future work: a CRM for OA, higher-frequency SML sampling across bloom events, and molecular characterisation of OA.

5 Conclusions

In summary, direct measurements indicate that the dynamics of OA concentrated in the SML influence near-surface pH, with a magnitude and timing that correspond to the vertical pH anomaly across bloom phases. Practically, we treat SML and ULW as paired observables: we measure OA together with NDIC, NTA, and pH, using co-time sampling, and report the OA EF alongside ΔpH so that layer contrasts are comparable across bloom phases. NDIC vs. NTA vectors identify phase-dominant biological processes, allowing bloom-driven inputs, reflected here as OA, to be distinguished from baseline conditions. Conceptually, a three-layer view, air-SML-ULW, locates where changes arise in organic-rich, biologically active waters and helps avoid attributing pH variability solely to processes beneath the SML. Looking ahead, the priorities are clear: developing a certified reference material for direct OA measurements is necessary to validate the concentration across laboratories, resolve the speciation of the active organic pool contributing to OA, and test the three-layer representation in natural environments. Together, these steps will integrate SML OA into observing systems and models, providing a practical framework to refine estimates of air-sea CO_2 in organic-rich, biologically active marine environments.

From these observations, a clear biogeochemical progression emerges from the mesocosm-induced phytoplankton bloom. NDIC vs. NTA vectors revealed a clear succession of dominant biological processes: photosynthetic drawdown at bloom onset,

https://doi.org/10.5194/egusphere-2025-5265
Preprint. Discussion started: 10 November 2025
© Author(s) 2025. CC BY 4.0 License.

mid-bloom phase restructuring with contributions from calcification and photosynthesis, and respiration-dominated when the bloom decayed. In line with previous studies, bloom phases likely released and transformed organic matter in the SML. Based on established literature and the observed dominant biological processes, these releases are expected to include extracellular polymeric substances such as acidic polysaccharides, humic-like material, and proteinaceous compounds. Subsequent microbial processing further enriches proton-active groups. Under bloom-driven organic production, OA in the SML was persistently higher than in the ULW and peaked at the transitions between bloom phases, while the SML and ULW pH difference narrowed and at times inverted. The coupled progression of SML OA and pH is consistent with a role for SML OA in modulating near-SML acid-base conditions: when enrichment was strong (EF above approximately 3), ΔpH approached or fell below zero, indicating that accumulated proton-active organics at the SML modified near-SML acid-base conditions and, episodically, influenced pH in the ULW. In summary, the bloom's biological sequence supplies and transforms organics, and the SML concentrates the proton-active OA fraction of TA, and this accumulation is reflected in the vertical pH anomalies between both layers. Understanding these dynamics brings OA into view as an active component of the MCS, essential for improving predictions of air-sea CO_2 exchange and acid-base system that links biology, chemistry and physics into the climate context.

6 Author contribution

Cortés Espinoza led the work of this manuscript, such as conceptualisation, methodology, investigation, formal analysis, visualisation, data curation, writing and provided the original draft for the co-authors. Würst A. developed and validated adjustments and improving the closed-cell titration for total alkalinity to measure the organic alkalinity (methodology, validation, review and editing). López-Puertas A. performed laboratory measurements of dissolved inorganic carbon, total alkalinity and organic alkalinity, and assembled the database. Waska H. supervised interpretation of dissolved organic matter and related compounds (supervision, conceptualisation, writing – review and editing). Wurl designed and coordinated the mesocosm experiment and logistics, and provided supervision and resources (conceptualisation, project administration, resources, supervision, funding acquisition). Ribas-Ribas and Hernández-Ayón J. M. guided the overall manuscript narrative and interpretation regarding to the marine carbon system. All authors discussed the results and approved the final manuscript.

7 Competing interests

The authors declare that they have no conflict of interest.

8 Special Issue Statement

This article is part of the special issue: Biogeochemical processes and air-sea exchange in the sea-surface microlayer (BASS).

https://doi.org/10.5194/egusphere-2025-5265
Preprint. Discussion started: 10 November 2025
© Author(s) 2025. CC BY 4.0 License.

9 Acknowledgements

We thank the German Research Foundation (DFG) for funding the BASS project. We are grateful to Riaz Bibi and Carola Lehners for coordinating the mesocosm study and the BASS project, and for providing a comprehensive overview of the study and its biogeochemical results. We thank Michael Novak and Rüdiger Röttgers (BASS SP1.3) for providing chlorophyll *a* concentration data, and Claudia Thölen and Jochen Wollschläger (BASS SP1.3) for providing FerryBox data. We also thank Henry Ovri and Jürgen Markmann (Helmholtz Center Hereon) for preparing and providing images that enabled the identification of *E. huxleyi*. We also thank to Carsten Rauch who provide the pH SML data used from the micro-profiles. We are especially indebted to everyone involved in conducting the mesocosm study, in particular Carola Lehners and Michaela Gerriets, for their enormous effort in making the study possible. Last but not least, we thank Jasper Zöbelein for the preparation of the artificial seawater used in the OA direct quantification.

10 Financial support

This research was supported by the project "Biogeochemical processes and Air–sea exchange in the Sea-Surface microlayer (BASS)", which was funded by the German Research Foundation (DFG) under Grant No 451574234.

https://doi.org/10.5194/egusphere-2025-5265
Preprint. Discussion started: 10 November 2025
© Author(s) 2025. CC BY 4.0 License.

References

Alldredge, A. L., Passow, U., and Logan, B. E.: The abundance and significance of a class of large, transparent organic particles in the ocean, Deep-Sea Res. Part I Oceanogr. Res. Pap., 40, 1131-1140, https://doi.org/10.1016/0967-0637(93)90129-Q, 1993.

Bakker, D. C. E., Pfeil, B., Smith, K., Hankin, S., Olsen, A., Alin, S. R., Cosca, C., Harasawa, S., Kozyr, A., Nojiri, Y., O'Brien, K. M., Schuster, U., Telszewski, M., Tilbrook, B., Wada, C., Akl, J., Barbero, L., Bates, N. R., Boutin, J., Bozec, Y., Cai, W. J., Castle, R. D., Chavez, F. P., Chen, L., Chierici, M., Currie, K., De Baar, H. J. W., Evans, W., Feely, R. A., Fransson, A., Gao, Z., Hales, B., Hardman-Mountford, N. J., Hoppema, M., Huang, W. J., Hunt, C. W., Huss, B., Ichikawa, T., Johannessen, T., Jones, E. M., Jones, S. D., Jutterström, S., Kitidis, V., Körtzinger, A., Landschützer, P., Lauvset, S. K., Lefèvre, N., Manke, A. B., Mathis, J. T., Merlivat, L., Metzl, N., Murata, A., Newberger, T., Omar, A. M., Ono, T., Park, G. H., Paterson, K., Pierrot, D., Ríos, A. F., Sabine, C. L., Saito, S., Salisbury, J., Sarma, V. V. S. S., Schlitzer, R., Sieger, R., Skjelvan, I., Steinhoff, T., Sullivan, K. F., Sun, H., Sutton, A. J., Suzuki, T., Sweeney, C., Takahashi, T., Tjiputra, J., Tsurushima, N., Van Heuven, S. M. A. C., Vandemark, D., Vlahos, P., Wallace, D. W. R., Wanninkhof, R., and Watson, A. J.: An update to the Surface Ocean CO_2 Atlas (SOCAT version 2), Earth Syst. Sci. Data, 6, 69-90, 10.5194/essd-6-69-2014, 2014.

Benson, N. U., Adedapo, A.E., Eritobor, A.L., Udosen, E.D.: Total dissolved inorganic carbon and physicochemical characteristics of surface microlayer and upper mixed layer water from Lagos Lagoon, Nigeria, Glob. NEST J., 17, 334-343, 2015.

Bibi, R., Ribas-Ribas, M., Jaeger, L., Lehners, C., Gassen, L., Cortés, E., Wollschläger, J., Thölen, C., Waska, H., Zöbelein, J., Brinkhoff, T., Athale, I., Röttgers, R., Novak, M., Engel, A., Barthelmeß, T., Karnatz, J., Reinthaler, T., Spriahailo, D., Friedrichs, G., Schäfer, F., and Wurl, O.: Biogeochemical Dynamics of the Sea-Surface Microlayer in a Multidisciplinary Mesocosm Study, Biogeosciences, 10.5194/egusphere-2025-1773, 2025.

Cai, W.-J., Wang, Y., and Hodson, R. E.: Acid-Base Properties of Dissolved Organic Matter in the Estuarine Waters of Georgia, USA, Geochim. Cosmochim. Acta, 62, 473-483, https://doi.org/10.1016/S0016-7037(97)00363-3, 1998.

Dickson, A. G.: An exact definition of total alkalinity and a procedure for the estimation of alkalinity and total inorganic carbon from titration data, Deep-Sea Res. Part I Oceanogr. Res. Pap., 28, 609-623, https://doi.org/10.1016/0198-0149(81)90121-7, 1981.

Dickson, A. G.: Thermodynamics of the dissociation of boric acid in synthetic seawater from 273.15 to 318.15 K, Deep-Sea Res. Part I Oceanogr. Res. Pap., 37, 755-766, https://doi.org/10.1016/0198-0149(90)90004-F, 1990.

Dickson, A. G. S., C.L. and Christian, J.R.: Guide to best practices for ocean CO_2 measurements, PICES Special Publication, 3, North Pacific Marine Science Organization, Sidney, British Columbia, 191 pp., https://doi.org/10.25607/OBP-1342, 2007.

Engel, A. and Passow, U.: Carbon and nitrogen content of transparent exopolymer particles (TEP) in relation to their Alcian Blue adsorption, Mar. Ecol. Prog. Ser., 219, 1-10, 10.3354/meps219001, 2001.

Friedlingstein, P., O'Sullivan, M., Jones, M. W., Andrew, R. M., Hauck, J., Landschützer, P., Le Quéré, C., Li, H., Luijkx, I. T., Olsen, A., Peters, G. P., Peters, W., Pongratz, J., Schwingshackl, C., Sitch, S., Canadell, J. G., Ciais, P., Jackson, R. B., Alin, S. R., Arneth, A., Arora, V., Bates, N. R., Becker, M., Bellouin, N., Berghoff, C. F., Bittig, H. C., Bopp, L., Cadule, P., Campbell, K., Chamberlain, M. A., Chandra, N., Chevallier, F., Chini, L. P., Colligan, T., Decayeux, J., Djeutchouang, L. M., Dou, X., Duran Rojas, C., Enyo, K., Evans, W., Fay, A. R., Feely, R. A., Ford, D. J., Foster, A., Gasser, T., Gehlen, M., Gkritzalis, T., Grassi, G., Gregor, L., Gruber, N., Gürses, Ö., Harris, I., Hefner, M., Heinke, J., Hurtt, G. C., Iida, Y., Ilyina, T., Jacobson, A. R., Jain, A. K., Jarníková, T., Jersild, A., Jiang, F., Jin, Z., Kato, E., Keeling, R. F., Klein Goldewijk, K., Knauer, J., Korsbakken, J. I., Lan, X., Lauvset, S. K., Lefèvre, N., Liu, Z., Liu, J., Ma, L., Maksyutov, S., Marland, G., Mayot, N., McGuire, P. C., Metzl, N., Monacci, N. M., Morgan, E. J., Nakaoka, S.-I., Neill, C., Niwa, Y., Nützel, T., Olivier, L., Ono, T., Palmer, P. I., Pierrot, D., Qin, Z., Resplandy, L., Roobaert, A., Rosan, T. M., Rödenbeck, C., Schwinger, J., Smallman, T. L., Smith, S. M., Sospedra-Alfonso, R., Steinhoff, T., Sun, Q., Sutton, A. J., Séférian, R., Takao, S., Tatebe, H., Tian, H., Tilbrook, B., Torres, O., Tourigny, E., Tsujino, H., Tubiello, F., Van Der Werf, G., Wanninkhof, R., Wang, X., Yang, D., Yang, X., Yu, Z., Yuan, W., Yue, X., Zaehle, S., Zeng, N., and Zeng, J.: Global Carbon Budget 2024, Earth Syst. Sci. Data, 17, 965-1039, 10.5194/essd-17-965-2025, 2025.

Friis, K., Körtzinger, A., and Wallace, D. W. R.: The salinity normalization of marine inorganic carbon chemistry data, Geophys. Res. Lett., 30, n/a-n/a, 10.1029/2002gl015898, 2003.

https://doi.org/10.5194/egusphere-2025-5265
Preprint. Discussion started: 10 November 2025
© Author(s) 2025. CC BY 4.0 License.

Gong, H., Zhang, Z., Zhang, C., Liu, L., and Xing, L.: Multilayer distribution of carbon dioxide system in surface water of the Yellow Sea in spring, Chin. J. Oceanol. Limnol., 25, 1-15, 10.1007/s00343-007-0001-4, 2007.
Harvey, G. W. and Burzell, L. A.: A SIMPLE MICROLAYER METHOD FOR SMALL SAMPLES1, Limnology and Oceanography, 17, 156-157, 10.4319/lo.1972.17.1.0156, 1972.
Hernández-Ayón, J. M., Zirino, A., Dickson, A. G., Camiro-Vargas, T., and Valenzuela-Espinoza, E.: Estimating the contribution of organic bases from microalgae to the titration alkalinity in coastal seawaters, Limnol. Oceanogr., 5, 225-232, 10.4319/lom.2007.5.225, 2007.
Johnson, K. M., King, A. E., and Sieburth, J. M.: Coulometric TCO_2 analyses for marine studies; an introduction, Mar. Chem., 16, 61-82, https://doi.org/10.1016/0304-4203(85)90028-3, 1985.
Kerr, D. E., Turner, C., Grey, A., Keogh, J., Brown, P. J., and Kelleher, B. P.: OrgAlkCalc: Estimation of organic alkalinity quantities and acid-base properties with proof of concept in Dublin Bay, Mar. Chem., 251, 104234, 2023.
Kim, H. C. and Lee, K.: Significant contribution of dissolved organic matter to seawater alkalinity, Geophys. Res. Lett., 36, 10.1029/2009gl040271, 2009.
Ko, Y. H., Lee, K., Eom, K. H., and Han, I.-S.: Organic alkalinity produced by phytoplankton and its effect on the computation of ocean carbon parameters, Limnol. Oceanogr., 61, 1462-1471, https://doi.org/10.1002/lno.10309, 2016.
Kuliński, K., Schneider, B., Hammer, K., Machulik, U., and Schulz-Bull, D.: The influence of dissolved organic matter on the acid-base system of the Baltic Sea, J. Mar. Syst., 132, 106-115, https://doi.org/10.1016/j.jmarsys.2014.01.011, 2014.
Middelburg, J. J., Soetaert, K., and Hagens, M.: Ocean Alkalinity, Buffering and Biogeochemical Processes, Rev. Geophys., 58, 10.1029/2019rg000681, 2020.
Millero, F. J., Byrne, R. H., Wanninkhof, R., Feely, R., Clayton, T., Murphy, P., and Lamb, M. F.: The internal consistency of CO_2 measurements in the equatorial Pacific, Mar. Chem., 44, 269-280, https://doi.org/10.1016/0304-4203(93)90208-6, 1993.
Moreno-Polo, K., Tobón-Monsalve, D., Florez-Leiva, L., Lehners, C., Wurl, O., Pacheco, W., and Ribas-Ribas, M.: Distribution of surfactants in the sea-surface microlayer across a tropical estuarine system in Caribbean Colombia, Estuar. Coast. Shelf Sci., 320, 109291, https://doi.org/10.1016/j.ecss.2025.109291, 2025.
Muller, F. L. L. and Bleie, B.: Estimating the organic acid contribution to coastal seawater alkalinity by potentiometric titrations in a closed cell, Anal. Chim. Acta, 619, 183-191, https://doi.org/10.1016/j.aca.2008.05.018, 2008.
Mustaffa, N. I. H., Ribas-Ribas, M., Banko-Kubis, H. M., and Wurl, O.: Global reduction of *in situ* CO_2 transfer velocity by natural surfactants in the sea-surface microlayer, Proc. R. Soc. A Math. Phys. Eng. Sci., 476, 20190763, 10.1098/rspa.2019.0763, 2020.
Orr, J. C., Fabry, V. J., Aumont, O., Bopp, L., Doney, S. C., Feely, R. A., Gnanadesikan, A., Gruber, N., Ishida, A., Joos, F., Key, R. M., Lindsay, K., Maier-Reimer, E., Matear, R., Monfray, P., Mouchet, A., Najjar, R. G., Plattner, G.-K., Rodgers, K. B., Sabine, C. L., Sarmiento, J. L., Schlitzer, R., Slater, R. D., Totterdell, I. J., Weirig, M.-F., Yamanaka, Y., and Yool, A.: Anthropogenic ocean acidification over the twenty-first century and its impact on calcifying organisms, Nature, 437, 681-686, 10.1038/nature04095, 2005.
Paasche, E.: Coccolith Formation, Nature, 193, 1094-1095, 10.1038/1931094b0, 1962.
Passow, U.: Transparent exopolymer particles (TEP) in aquatic environments, Prog. Oceanogr., 55, 287-333, 10.1016/s0079-6611(02)00138-6, 2002.
Pereira, R., Schneider-Zapp, K., and Upstill-Goddard, R. C.: Surfactant control of gas transfer velocity along an offshore coastal transect: results from a laboratory gas exchange tank, Biogeosciences, 13, 3981-3989, 10.5194/bg-13-3981-2016, 2016.
Perez, F. F. and Fraga, F.: Association constant of fluoride and hydrogen ions in seawater, Mar. Chem., 21, 161-168, https://doi.org/10.1016/0304-4203(87)90036-3, 1987.
Ribas-Ribas, M., Helleis, F., Rahlff, J., and Wurl, O.: Air-Sea CO_2-Exchange in a Large Annular Wind-Wave Tank and the Effects of Surfactants, Front. Mar. Sci., 5, 10.3389/fmars.2018.00457, 2018.
Riley, J. P.: The occurrence of anomalously high fluoride concentrations in the North Atlantic, Deep-Sea Res. Part I Oceanogr. Res. Pap., 12, 219-220, 10.1016/0011-7471(65)90027-6, 1965.
Song, S., Bellerby, R. G. J., Wang, Z. A., Wurgaft, E., and Li, D.: Organic Alkalinity as an Important Constituent of Total Alkalinity and the Buffering System in River-To-Coast Transition Zones, J. Geophys. Res. Oceans., 128, 10.1029/2022jc019270, 2023.
Takahashi, T., Sutherland, S. C., Wanninkhof, R., Sweeney, C., Feely, R. A., Chipman, D. W., Hales, B., Friederich, G., Chavez, F., Sabine, C., Watson, A., Bakker, D. C. E., Schuster, U., Metzl, N., Yoshikawa-Inoue, H., Ishii, M., Midorikawa,

https://doi.org/10.5194/egusphere-2025-5265
Preprint. Discussion started: 10 November 2025
© Author(s) 2025. CC BY 4.0 License.

T., Nojiri, Y., Körtzinger, A., Steinhoff, T., Hoppema, M., Olafsson, J., Arnarson, T. S., Tilbrook, B., Johannessen, T., Olsen, A., Bellerby, R., Wong, C. S., Delille, B., Bates, N. R., and de Baar, H. J. W.: Climatological mean and decadal change in surface ocean pCO_2, and net sea-air CO_2 flux over the global oceans, Deep-Sea Res. Part II Top. Stud. Oceanogr., 56, 554-577, https://doi.org/10.1016/j.dsr2.2008.12.009, 2009.

Wurl, O. and Holmes, M.: The gelatinous nature of the sea-surface microlayer, Mar. Chem., 110, 89-97, https://doi.org/10.1016/j.marchem.2008.02.009, 2008.

Wurl, O., Wurl, E., Miller, L., Johnson, K., and Vagle, S.: Formation and global distribution of sea-surface microlayers, Biogeosciences, 8, 121-135, 10.5194/bg-8-121-2011, 2011.

Yang, B., Byrne, R. H., and Lindemuth, M.: Contributions of organic alkalinity to total alkalinity in coastal waters: A spectrophotometric approach, Mar. Chem., 176, 199-207, https://doi.org/10.1016/j.marchem.2015.09.008, 2015.

Zeebe, R. E. and Wolf-Gladrow, D.: CO_2 in seawater: equilibrium, kinetics, isotopes, Gulf Professional Publishing2001.

Zhang, Z.: Direct determination of thickness of sea surface microlayer using a pH microelectrode at original location, Sci. China Ser. B: Chem, 46, 339, 10.1360/02yb0192, 2003.